Community behaviors of bacteria in flow: Divergent roles for transport and collective morphology

Kelsey M. Hallinen[1], Steven P. Bodine[2], Howard A. Stone[3], Tom W. Muir[2], Ned S. Wingreen[4,5], and Zemer Gitai[5*]

[1]Department of Physics, Princeton University
[2]Department of Chemistry, Princeton University
[3]Department of Mechanical and Aerospace Engineering, Princeton University
[4]Lewis-Sigler Institute for Integrative Genomics, Princeton University
[5]Department of Molecular Biology, Princeton University

Abstract

Fluid flows are dominant features of many bacterial environments, and flow can often impact bacterial behaviors in unexpected ways[1–3]. For example, the most common types of cardiovascular infections are heart valve colonization by Gram-positive bacteria like *Staphylococcus aureus* and *Enterococcus faecalis* (endocarditis)[4,5]. This behavior is seemingly paradoxical because heart valves experience high shear rates that would naively be expected to reduce colonization. To ascertain the mechanisms underlying the ability of these bacteria to preferentially colonize higher shear rate environments, we developed a microfluidic system to quantify the effect of flow conditions on the colonization of *S. aureus* and *E. faecalis*. We find that the preferential colonization in high flow of both species is not specific to heart valves and can be found in simple configurations lacking any host factors. Surprisingly, experimental and computational studies reveal that the two species achieve this behavior via distinct mechanisms. *S. aureus* grows in cell clusters and produces a dispersal signal whose transport is affected by shear rate. Meanwhile, *E. faecalis* grows in linear chains whose mechanical properties result in less dispersal in the presence of higher shear force. In addition to establishing two divergent mechanisms by which these bacteria each preferentially colonize high-flow environments, our findings highlight the importance of understanding bacterial behaviors at the level of collective interactions among cells. These results suggest that distinct microcolony morphologies have previously unappreciated costs and benefits in different environments, like those introduced by fluid flow.

Introduction

Bacterial populations experience a range of complex environments in their natural settings[2]. For example, within a host, bacteria must contend with fluid flows such as those found in the cardiovascular system[6]. Fluid flow can significantly impact how bacteria interact with one another or with the surfaces that they colonize[7–13]. Recent studies have begun to examine the effect of flow on single-cell bacterial behaviors like growth[14,15] and adhesion[16–20]. For example, catch bonds can enable individual bacterial cells to adhere to epithelial surfaces more strongly in flow[21]. However, these single-cell mechanisms are often not widely conserved. Furthermore, in natural settings bacteria are typically in dynamic multicellular communities and the effects of complex environments on these cell collectives are underexplored.

One example of a counterintuitive bacterial behavior in the presence of flow comes from clinical reports of infective endocarditis. Infective endocarditis is an infection in the heart, where bacteria are most commonly reported to colonize heart valves[4,5,20,22,23]. These infections are difficult to treat and even with the use of antibiotics surgery is often needed to replace infected valves[24]. From the perspective of fluid mechanics, the valves have the narrowest cross-sectional areas in the heart, causing them to have the fastest flow speed[6]. These observations lead to an intriguing paradox: higher flow speeds would naively be thought to reduce surface colonization, so how might bacteria preferentially colonize the regions of the heart with the highest flow conditions?

Here we sought to directly examine the effects of flow on how bacteria that cause endocarditis colonize surfaces. To this end, we studied two different bacterial species commonly implicated in endocarditis infections, Methicillin-resistant *Staphylococcus aureus* (MRSA) and

64 *Enterococcus faecalis*, and imaged their surface colonization within microfluidic devices. Our
65 results demonstrate that these bacteria preferentially colonize surfaces in high shear conditions,
66 even when the surface is abiotic, suggesting that this counterintuitive behavior is driven by the
67 bacteria themselves. Elucidating how the two species preferentially adhere in high shear
68 environments reveal two divergent mechanisms that rely on their distinct microcolony
69 morphologies and are driven by either transport of signaling molecules or mechanical responses
70 to flow.
71

72 **Results**

73 **Bacterial populations exhibit counterintuitive adhesion behaviors in microfluidic studies**

74 To assess the impact of flow on bacteria in the absence of host factors, we examined the
75 colonization of glass coverslips for both *S. aureus* (USA300 MRSA) and *E. faecalis* (OG1RF) in
76 untreated microfluidic channels (Fig. 1A). For all experiments described below, cells were
77 seeded into the channel and allowed to adhere to the glass coverslip before we flowed in sterile
78 media, such that no new cells were introduced to the system once flow began. In any given flow
79 system, there is a flow rate (volume/time) and a typical speed (flow rate divided by the cross-
80 sectional area of the flow). The fluid speed is zero at the boundaries, so cells at the surface
81 typically experience a flow (or velocity) profile that increases with distance from the wall.
82 Hence, the cells attached to a wall experience a shear rate (units 1/second). For a given
83 configuration, higher flow rates correspond to higher shear rates. The shear rate in heart valves is
84 estimated to be roughly 100/s (estimated from [25,26] as detailed in the supplement). For each
85 species, we thus initially examined two shear rates: a low shear rate of 40/s (low flow) and a high
86 shear rate of 400/s (high flow). Despite the naive expectation that higher shear rate should hinder

87 colonization, by the end of our experiments we observed that more bacteria colonized the surface
88 for both *S. aureus* and *E. faecalis* (Fig. 1). In our timelapse movies we observed that the
89 attachment of new cells to the surface was relatively rare in both high flow and low flow for both
90 species (Movie S1-4). Furthermore, analysis of single cell doubling time showed no significant
91 difference between the low and high flow conditions for either species, indicating that the
92 differences in colonization cannot be explained by differences in growth rate (Fig. 1B). Since the
93 differences between high and low flow could not be explained by differences in attachment or
94 growth, we hypothesized that they are likely driven by differences in detachment.
95
96 Examining the dynamics of *S. aureus* colonization, we found that for the first several hours
97 surface colonization increased at a similar rate in both low and high flow. During these early
98 timepoints we observed that the bacteria formed small microcolonies with a clustered
99 morphology. After roughly 3 hours, however, we began to observe a striking difference between
100 the low and high flow conditions. At these later timepoints, *S. aureus* continued to colonize more
101 and more of the surface in the high flow conditions. But in the low flow condition, *S. aureus*
102 began to disperse from the surface, leading to a decrease in coverage and smaller microcolony
103 clusters. Image analysis of the fraction of the surface area covered by bacteria confirmed that in
104 high flow colonization proceeded to monotonically increase, but that in low flow, colonization
105 increased for the first 3 hours and then exhibited increasing dispersal for the rest of the
106 experiment (Fig. 1C-E).
107
108 Examining the dynamics of *E. faecalis* colonization revealed a different pattern from that of *S.*
109 *aureus*. Throughout the experiments we found that *E. faecalis* grew as microcolonies with a

110 linear chained morphology (Fig. 1F-G). In both low and high flow, *E. faecalis* surface
111 colonization increased mostly monotonically, but the rate of the increased surface colonization
112 was consistently lower in low flow than in high flow conditions (Fig. 1F-H). Together, these
113 experiments suggest that the surface colonization of both *E. faecalis* and *S. aureus* is
114 counterintuitively greater in high flow than in low flow. While changes in detachment rate
115 appear to underlie both behaviors, the two species likely respond to flow differently, as they
116 exhibit distinct colonization kinetics.
117

118 **Transport of a signaling molecule drives the *S. aureus* flow response**

119 To begin to understand the mechanisms by which flow might affect colonization, we first
120 considered the possibility that the bacterial cells might be responding to changes in their
121 chemical environments. Bacteria are known to produce and consume various molecules whose
122 concentration changes can activate or repress signaling pathways that can alter the expression of
123 factors like adhesins[27] that influence colonization[24]. To test whether such chemical changes
124 could explain the behaviors we observed for *S. aureus* and *E. faecalis,* we generated
125 "conditioned" media where each bacterial species was grown overnight, sterile-filtered to
126 remove intact bacterial cells, and diluted 1:1 with fresh media to ensure access to the nutrients
127 necessary for growth. We then examined bacterial colonization in the presence of high shear rate
128 conditions (high flow) as above, but switched the media halfway through the experiment from
129 fresh to conditioned media. In the presence of high flow, conditioned media caused opposite
130 effects on *S. aureus* and *E. faecalis.* Specifically, conditioned media decreased colonization for
131 *S. aureus,* leading to colonization in high flow that more closely resembled *S. aureus*
132 colonization in low flow (Fig. 2A, B). Meanwhile, for *E. faecalis,* conditioned media increased

133 colonization, exacerbating the difference between high and low flow (Fig. 2C, D). Thus, the
134 differential responses in the kinetics of *S. aureus* and *E. faecalis* colonization in flow correlate
135 with differences in these species' responses to conditioned media.
136
137 One way in which bacteria are known to respond to conditioned media is through quorum
138 sensing (QS). In QS, bacteria both secrete and sense signaling molecules called autoinducers. In
139 well-mixed environments, autoinducer concentration correlates with bacterial cell density,
140 thereby enabling bacteria to drive collective behaviors. Flow can influence QS by affecting
141 autoinducer transport, here defined as the movement of signaling molecule into or out of the
142 bacterial biofilm by diffusion or advection by flow[28–30]. To determine whether the interactions
143 between flow and QS could help explain the flow-dependent surface colonization of *S. aureus*
144 and *E. faecalis*, we developed a model in which the number of cells on a surface changes as a
145 function of cell growth, attachment and detachment, and autoinducer concentration changes as a
146 function of the number of cells, transport, and diffusion (Fig. 2E). In this model autoinducer
147 concentration can positively or negatively influence attachment (the parameter β), but
148 autoinducer concentration does not affect growth because we observed no changes in growth rate
149 in our experiments (Fig. 1B).
150
151 Exploring the parameters of our transport-dependent colonization model revealed that whether
152 quorum sensing positively or negatively influences attachment (the sign of β) was sufficient to
153 explain some, but not all, of the dynamics we observed experimentally. In all cases the system
154 starts with low cell numbers, such that the effect of quorum sensing becomes more pronounced
155 at later times. Regardless of the sign of β, increased shear rate led to more autoinducer transport

156 (represented by the transport term, q) and thus less autoinducer accumulation. When β is
157 negative and shear rate is low, growth rate initially dominates so cell numbers increase at early
158 timepoints, but after cell density increases, autoinducer accumulates and inhibits cell attachment
159 to an extent that eventually overwhelms growth and decreases cell numbers. In contrast, when β
160 is negative and shear rate is high, autoinducer accumulates less and never overtakes growth, such
161 that cell number steadily increases throughout the experiment (Fig. 2F). These results suggest
162 that the effects of shear rate on QS can explain the behaviors we observe for *S. aureus* in which
163 colonization initially increases in both high and low flow but then later diverges, continuing to
164 increase in high flow but decreasing in low flow. Consistent with a negative β being appropriate
165 for modeling *S. aureus* colonization, quorum sensing has previously been shown to downregulate
166 surface adhesins[31–33] and here we experimentally confirm that conditioned media reduces *S.*
167 *aureus* colonization (Fig. 2A-B).
168
169 We also sought to determine if our transport-dependent colonization model can explain the
170 colonization behavior of *E. faecalis.* Since *E. faecalis* colonization is not seen to decrease over
171 time in any conditions, the negative β model that works for *S. aureus* does not work for *E.*
172 *faecalis.* QS is known to stimulate *E. faecalis* adhesion[34] and here we observed that conditioned
173 media enhanced colonization (Fig. 2C-D). We thus examined colonization dynamics in our
174 model when β is positive and quorum sensing stimulates cell attachment. In this case, we found
175 that cell number always increased over time but did so more rapidly in low flow than in high
176 flow because autoinducer accumulates more and thus more strongly promotes attachment in low
177 flow (Fig. 2G). In contrast, our experimental results demonstrated that *E. faecalis* cells colonized
178 more in high flow than in low flow (Fig. 1F-H). These results suggest that the transport-

179 dependent colonization model is not sufficient to explain the colonization behavior of *E. faecalis*
180 in flow.
181
182 To directly test our predictions that QS can explain the effects of flow on the colonization of *S.*
183 *aureus* but not *E. faecalis,* we synthesized the primary autoinducer signaling molecule from each
184 species: autoinducing peptide (AIP), which activates *agr* quorum sensing in *S. aureus* and
185 gelatinase biosynthesis-activating pheromone (GBAP), which activates *fsr* quorum sensing in *E.*
186 *faecalis*). Addition of AIP to *S. aureus* decreased colonization and caused cell coverage in high
187 flow to more closely resemble that in low flow (Fig. 2H, I). By contrast, growth of *E. faecalis*
188 under flow conditions with the addition of GBAP increased colonization, expanding the
189 colonization difference between the low and high flow conditions (Fig. 2J, K). These results
190 were consistent with our model's predictions.
191
192 **Mechanics of chained cells in flow drive *E. faecalis* colonization dynamics**
193 Because quorum sensing can explain how colonization dynamics depend on flow for *S. aureus*
194 but not for *E. faecalis,* we sought to determine the mechanism by which high flow enhances *E.*
195 *faecalis* colonization. One striking difference between *S. aureus* and *E. faecalis* is that they have
196 distinct growth patterns that result in different microcolony morphologies. *S. aureus* cells divide
197 in alternating division planes[35], resulting in rounded microcolonies of closely clustered cells. By
198 contrast, *E. faecalis* cells divide along a single plane[36], resulting in linear microcolonies of cell
199 chains. We hypothesized that the mechanical effects of flow on this chained microcolony
200 morphology might help explain the flow dependence of *E. faecalis*. In the presence of flow, a
201 cell chain that is anchored to the surface at one end will experience a torque produced by the

202 shear force from the flow. The higher the flow rate, the larger this shear force becomes,
203 increasing the torque and pushing the chain closer to the surface. Shear force can be increased
204 independently of shear rate by increasing the viscosity of the fluid. To test how *E. faecalis*
205 colonization depends on shear force, we thus increased the viscosity of the bacterial media
206 roughly 5-fold by supplementation with 10% ficoll, a polymer that does not affect bacterial
207 growth. We found that this increased viscosity significantly enhanced *E. faecalis* colonization at
208 equivalent shear rates, indicating that its colonization is indeed dependent on shear force (Fig. 3,
209 A-B).
210
211 We next sought to experimentally determine if increased shear force pushes *E. faecalis* chains
212 more towards the surface (as illustrated in Fig. 3C). We observed that cell chains in high shear
213 force conditions were more sharply in focus in our images, suggesting that they were closer to
214 the focal plane that was positioned at the surface in these experiments (Fig. 3D). To quantify this
215 effect, we measured the fraction of total cells in focus. Relative to low flow, increasing shear
216 force by either increasing shear rate or viscosity resulted in a clear increase in the fraction of
217 cells in focus (Fig. 3E). We also noted that the fraction of cells in focus increased over time
218 during each experiment (Fig. 3E). This result is consistent with our hypothesis, as cell chains
219 elongate during the experiment and longer chains experience higher torque.
220
221 To more fully capture the mechanical responses of *E. faecalis* chains to flow, we developed a
222 mechanics-dependent colonization model (Fig. 3F). This is a 2D agent-based model in which
223 cells are agents that can be connected to one another to form chains. Chains are allowed to grow,
224 as growth continues during our experiments, and each cell can independently attach or detach

225 from the surface. The attachment probability depends on a cell's distance from the surface, while
226 detachment probability increases if neighboring cells are detached. Moreover, the connection
227 between two neighboring cells in a chain can stochastically break. A chain is considered to be
228 attached to the surface if any of its cells are attached. To mimic the dynamics observed
229 experimentally, chains begin with an origin cell attached to the surface and subsequent cells are
230 attached at the end of the chain by a stiff spring with a bending energy that keeps the cells in a
231 relatively straight line. An additional force acting on the chains is a drag force that acts in the
232 horizontal direction to recapitulate the shear force from flow. We found that in our simulations,
233 increased flow rate increased the number of cells that attached to the surface (Fig. 3G),
234 recapitulating our experimental results with *E. faecalis.*
235
236 Closer examination of our simulations revealed that flow has a significant impact on the outcome
237 of chain breakage events. When a chain breaks, the part of the chain proximal to the ancestral
238 origin cell has the same probability of remaining attached regardless of the flow rate (Fig. 3I).
239 This can be explained by this portion of the chain having a high probability of being attached in
240 all cases (Fig. 3H). In contrast, the part of the chain distal to the origin cell has a higher
241 probability of remaining attached in high flow than in low flow (Fig. 3I). This can be explained
242 by the higher drag force pushing the cell chain closer to the surface and thus increasing the
243 probability that cells in the distal part of the chain will be attached to the surface (Fig. 3H).
244
245 To test the mechanics-dependent colonization model's prediction that chain breakages should
246 have flow-dependent outcomes, we analyzed chain breakage events from our experiments in
247 both high and low flow. Specifically, we quantified the fraction of breakages where the origin

248 cells or distal cells remained adhered after the break (Fig. 3J). As predicted, there was no
249 significant difference between the fraction of origin cells adhered following a breakage between
250 low and high flow conditions (Fig. 3K). However, there was a significant difference in distal
251 adherence, with more distal cells adhering in high flow than in low flow after a breakage event
252 (Fig. 3K). Examples of the differences in chain breakage outcomes in high and low flow are
253 shown in Movies S5-8. Together, our experiments and modeling suggest that high flow rates
254 mechanically push *E. faecalis* chains towards the surface, which results in increased colonization
255 by increasing attachment and thereby reducing cell dispersal upon chain breakage.
256
257 **Discussion:**
258 Fluid flow introduces complexities to bacterial dynamics that can result in unexpected emergent
259 behaviors. Here we elucidate two divergent mechanisms by which two different species
260 preferentially colonize surfaces in higher flow environments (Fig. 4A,B). Previous studies of
261 bacterial colonization in flow have primarily focused on the mechanisms by which single cells
262 adhere to surfaces, such as the catch bonds formed between Uropathogenic *Escherichia coli* and
263 the mannosylated surface of epithelial cells[21] or the mechanosensitive Type IV pili of
264 *Pseudomonas aeruginosa*[37,38]. By contrast, here we find that increased flow stimulates
265 colonization of both *S. aureus* and *E. faecalis* via distinct mechanisms that each function at the
266 multicellular scale. Both our experimental studies of colonization in varying flow and
267 conditioned media, and a biophysical transport-dependent colonization model, suggest that the
268 effects of flow on quorum sensing could explain the flow-dependent colonization of *S. aureus*
269 but not *E. faecalis.* Further experiments with synthesized quorum sensing autoinducers
270 confirmed that for *S. aureus,* but not *E. faecalis*, flow enhances colonization through a reduction

271 in QS signaling resulting from increased autoinducer transport. These results are consistent with
272 previous findings that activating quorum sensing circuits downregulates adhesin expression in *S.*
273 *aureus*[30,31,39] and that increased shear rates decrease quorum sensing signaling by increasing
274 autoinducer transport[30]. Importantly, whereas previous studies on quorum sensing in flow
275 suggested that flow negates the physiological impact of quorum sensing in many contexts, our
276 findings suggest that bacteria may harness the inhibition of quorum sensing in flow as a
277 beneficial adaptation to promote colonization. Additional studies inspired by this work will help
278 to determine the importance of interactions between multicellular signaling and flow in
279 physiologically-relevant environments.
280
281 In contrast to *S. aureus,* we found that mechanical effects and different multicellular morphology
282 were sufficient to explain how flow stimulates the colonization of *E. faecalis*. Altering fluid
283 viscosity suggested that the *E. faecalis* colonization effect depends upon shear force rather than
284 solely the shear rate, and agreement between experimental observations and a biophysical
285 mechanics-dependent colonization model confirmed our hypothesis. Specifically, we found that
286 the linear chains of cells produced by *E. faecalis* microcolonies experience a torque that is
287 proportional to viscous effects. Consequently, higher flow pushes the cells more towards the
288 surface, leading to increased attachment.
289
290 Interestingly, while *S. aureus* and *E. faecalis* achieve flow-dependent colonization in different
291 ways, both mechanisms do not operate on single cells but rather depend on the specific collective
292 morphologies of each species' microcolonies. The clustered multicellular morphology in which
293 *S. aureus* cells grow facilitates the local 3D signaling interactions that mediate quorum sensing.

294 Meanwhile, the linear multicellular morphology of *E. faecalis* produces a lever-like effect that
295 promotes the torque required for flow-dependent attachment.
296
297 Many studies of single-cell bacterial morphology have noted the importance of individual cell
298 shape[40–42], but our findings suggest that even when individual bacteria have cells of the same
299 shape, there can be adaptive benefits to the collective morphologies that form in their
300 multicellular microcolonies. Most bacterial species have highly stereotyped collective
301 morphologies, such that future studies will need to explore the costs and benefits of distinct
302 multicellular shapes in different environments. Beyond effects in flow, collective multicellular
303 morphology may lead to advantages or disadvantages in processes like horizontal gene transfer,
304 nutrient searching, competition in multispecies environments, or phage defense (Fig. 4C). For
305 example, cell clustering would lead to more interactions between cells within a local
306 neighborhood, perhaps driving easier DNA exchange or protection from competition of other
307 species, paralleling dynamics seen on a smaller length scale with enzyme clustering driving
308 metabolic responses[43]. Meanwhile, linear collective morphologies in which cells form chains
309 allow bacteria to increase their surface area to explore wider areas of their environments, perhaps
310 leading to advantages in nutrient acquisition or impacting the spread of phages. Thus, the
311 collective responses we have observed in flow not only introduce two divergent mechanisms for
312 the counterintuitive effect in which flow stimulates colonization, but also lead to further
313 implications for multicellular-scale bacterial responses in a wide array of environments.
314

319 ***Materials And Methods***

320 **Bacterial Strains and Growth Conditions**

321 *S. aureus* cells used in this study used the strain USA300 MRSA. *E. faecalis* studies were done
322 using the strain OG1RF, fluorescently labeled with the plasmid pBSU101-GFP[44] (generously
323 provided by the Wood Lab at the University of Michigan).

324

325 Media was prepared according to manufacturer recommendation. Overnight cultures were grown
326 in floor shakers at 37C in Luria-Bertani Miller (LB) Broth (BD Biosciences) for *S. aureus* or
327 Brain Heart Infusion (BHI) Broth (BD Biosciences) for *E. faecalis* following isolation of a single
328 colony from LB or BHI agar plates, respectively. For *E. faecalis* OG1RF, the plasmid pBSU101-
329 GFP was maintained with the addition of 120 μg/ml of the antibiotic Spectinomycin (Sigma) in
330 the plates as well as growth media.

331

332 Following overnight growth, cells were diluted in fresh media to an OD between 0.40 and 0.45
333 and loaded into plastic syringes with a 27G needle in preparation for microfluidic chip
334 experiments.

335

336 For conditioned media experiments, overnight cultures were centrifuged at 9000xg for 5 minutes
337 to pellet the cells. The supernatant was removed and filtered using 0.2 μm filter disks (Pall
338 Corporation) to ensure all cells had been removed. This filter sterilized overnight media was then
339 mixed 1:1 with fresh LB (*S. aureus*) or BHI (*E. faecalis*) to create our conditioned media. For
340 conditioned media experiments, we switched the syringes to conditioned media syringes from
341 fresh media following 3 hours of the flow run.

342

343 For *S. aureus* AIP experiments, synthesized AIP-I (obtained as described below) was added to
344 fresh LB to a final concentration of 50 nM. The LB supplemented with AIP was used for the
345 entire flow experiment. Similarly, for *E. faecalis* GBAP runs, synthesized GBAP was added to
346 fresh BHI to a final concentration of 50 nM. Again, the BHI supplemented with GBAP was used
347 for the entire 6-hour flow experiment.

348

349 For *E. faecalis* viscosity and shear force experiments, 10% ficoll (Sigma) was added to BHI.
350 This BHI + 10% ficoll media was used for the entire 6-hour experiment.

351

352 **AIP and GBAP Synthesis**

353 *AIP:* AIP-I was synthesized via a protocol adapted from Zhao *et al.* 2022[45]. Briefly, we
354 performed standard automated Fmoc-SPPS on a Liberty Blue microwave-assisted peptide
355 synthesizer (CEM), utilizing a DIC-Oxyma coupling strategy on a hydrazine derivatized Cl-
356 TCP(Cl)-ProTide resin (CEM). After SPPS, cleavage of the resin yielded a linear peptide with a
357 C-terminal hydrazide. This hydrazide was oxidized with 15 eq. of $NaNO_2$ in a 6 M guanidinium
358 hydrochloride buffer solution at pH 3. A peptide thioester was formed upon the addition of 15
359 eq. MESNa at pH 6.2. The MESNa thioester was purified by RP-HPLC and lyophilized. To
360 generate the cyclized final product, the peptide thioester was solubilized in PBS with 5 mM
361 TCEP at pH 7. AIP-I was purified again by RP-HPLC, lyophilized, and taken up in DMSO.
362 Concentration was determined by NMR relative to known standards.

363

364 *GBAP*: GBAP was synthesized via a protocol adapted from McBrayer *et al.* 2017[46]. Briefly,
365 GBAP was generated by Fmoc-SPPS using a HATU coupling strategy extending the chain from
366 Gln9 of the peptide. The unprotected side chain of Fmoc-Glu-Oall was coupled to a H-Rink
367 amide ChemMatrix® resin (Matrix Innovations). The peptide was extended to Asn2 by standard
368 Fmoc-SPPS. To the N-terminus was coupled Boc-Gln-OH to supply Gln1 and cap this chain of
369 the peptide. To add Met9 and Trp10 and form the ester linkage of the peptide lactone, the O-
370 trityl protecting group of Ser3 was first removed with 1% TFA. Fmoc-Met-OH (10 eq) was
371 coupled to the Ser3 side chain by a Steglich-type esterification, utilizing DIC (9.9 eq), DIEA (10
372 eq), and DMAP (0.5 eq). After validating the formation of the Met9 ester by LC-MS, Trp10 was
373 added by standard Fmoc-SPPS. The C-terminal Oalloc protecting group on Gln9 was removed
374 by treatment with 10 eq 1,3-dimethybarbituric acid and 0.3 eq
375 tetrakis(triphenylphosphine)palladium(0) in DCM. After repeating the Alloc deprotection, the Pd
376 catalyst was removed by washing with 1% sodium diethylthiocarbamate. On-resin cyclization
377 was performed with PyOxim (1.25 eq) and DIEA (2.5 eq). Cyclized product was cleaved from
378 the resin and purified by RP-HPLC. Pure products were lyophilized, taken up in DMSO, and
379 quantified by NMR.
380
381 **Microfluidic Devices**
382 Flow channels were designed in Blender and a 3D mold was printed by Protolabs (Maple Plain,
383 MN). Each chip had six channels that were 2 cm long x 500 μm wide x 100 μm tall with separate
384 inlet and outlet ports for each channel. Briefly, Polydimethylsiloxane (PDMS) was poured onto
385 the 3D mold, baked overnight, and then plasma-bonded to 22x44 mm #1.5 glass coverslips

386 (Avantor). Following this, the completed chips were baked overnight at 65C to complete the
387 bonding before use.
388
389 **Flow Experiments**
390 Microfluidic chips were prepared for flow experiments by adding inlet and outlet tubing (BD
391 Intramedic Polyethylene Tubing .015" ID 0.043" OD) and loading the channel with media before
392 addition of our diluted cells. Following cell addition, a plastic media-filled syringe with 27G
393 needle was connected to the inlet tubing and mounted on a syringe pump (New Era Pump
394 Systems, Inc.) and the outlet tubing was placed into a waste container to collect the outflow.
395 Following 15-20 minutes of initial attachment time, flow was turned on at one of two rates. For
396 high flow conditions corresponding to a shear rate 400/s, a flow rate of 20 μl/min was used. For
397 low flow conditions corresponding to a shear rate 40/s, a flow rate of 2 μl/min was used.
398
399 **Phase Contrast and Fluorescence Microscopy**
400 For all flow experiments, a Nikon 90i inverted microscope equipped with a 100x 1.4 N.A.
401 objective and with an incubator held at 37C was used. Microscope control and image acquisition
402 was done using NIS Elements (Nikon, version 4.60.00). Five positions spread along each
403 channel were chosen and the image plane was focused on the glass coverslip. Flow was turned
404 on following the first set of images. Images were then taken every 5 minutes for a total of 6
405 hours for both species. Phase contrast images were taken for all species. For *E. faecalis*,
406 fluorescent images were taken using a GFP filter. To obtain doubling time information (Fig 1B),
407 the same flow set up and microscopy filters were used, but images were taken every 2 minutes
408 for better doubling time resolution.

409

410 **Quantification of Cell Coverage**

411 Cell coverage analysis was completed using a custom image analysis macro in Fiji (software
412 available upon request). Briefly, for *S. aureus*, cell edges were found and contrast between the
413 edges and background was enhanced using a CLAHE filter. Images were thresholded to remove
414 background, binarized, and edges were filled in. Total cell coverage was determined by summing
415 the total pixel count of the binarized images. For *E. faecalis*, analysis was done using fluorescent
416 images to better capture the chains. Images were run through the CLAHE filter before having the
417 background subtracted and binarized. Once again, total cell coverage was then determined by
418 summing the total pixel count of the binarized images. The total coverage was normalized to the
419 first image for each experiment position, and then the normalized total coverage for all positions
420 of each experimental condition were averaged together. Error bars on these averages are reported
421 as standard error on the mean (SEM).

422

423 **Focus Analysis**

424 *E. faecalis* focus analysis was again completed with a custom pipeline in Fiji and MATLAB
425 (software available upon request, Mathworks, Natick, MA). Analysis began in Fiji, with the
426 phase contrast images CLAHE filtered followed by finding the edges of the cells. These edged
427 images were then loaded into MATLAB. The edges of out-of-focus cells were dim and could be
428 excluded by thresholding the images. The same threshold was used for all conditions. For each
429 time point in an experiment, the thresholded and non-thresholded images were binarized and the
430 total pixel value of each binarized image was calculated. The fraction in focus was then
431 calculated by dividing the thresholded image total by the non thresholded image. These results

were then normalized to the initial time point for each position and all positions for a specific condition were averaged together. Error bars are again reported as SEM.

Chain Breakage Analysis

For analysis of chain breakage outcomes, thirty breakage events were calculated by hand for low and high flow. Following a breakage, origin attachment and/or distal attachment was recorded. The fraction of events where origin or distal attachment was recorded was calculated by dividing the total number of times the breakage outcome was recorded by our total number of breakage observations (thirty). Error bars are SEM. Significance was determined used a paired t-test.

For simulations, anytime a breakage event was occurred, the outcome (origin and/or distal attachment) was recorded. Following the end of a chain simulation, these outcomes were recorded. For 100 chains in each simulation set, representing a 'position' along a simulated flow channel, the total outcomes of each were calculated and again the fractions were calculated, error bars are SEM, and significance was determined using a paired t-test.

Code Availability

Custom Fiji Macros and MATLAB code used for cell quantification and focus analysis of the microscopy data are freely available from the corresponding author upon request. Similarly, MATLAB code for both the transport-dependent colonization model and mechanics-dependent colonization model are freely available from the corresponding author upon request.

Data Availability

The data supporting the findings of the study are available in this article and its Supplementary Information. Additionally, the raw data that support the findings of this study are available from the corresponding author upon request.

457 **References**

458 1. Wheeler, J. D., Secchi, E., Rusconi, R. & Stocker, R. Not Just Going with the Flow: The
459 Effects of Fluid Flow on Bacteria and Plankton. *Annu Rev Cell Dev Biol* **35**, 213–237
460 (2019).

461 2. Persat, A. *et al.* The Mechanical World of Bacteria. *Cell* **161**, 988–997 (2015).

462 3. Gordon, V. D. & Wang, L. Bacterial mechanosensing: the force will be with you, always.
463 *J Cell Sci* **132**, jcs227694 (2019).

464 4. Cahill, T. J. & Prendergast, B. D. Infective endocarditis. *The Lancet* **387**, 882–893 (2016).

465 5. Cahill, T. J. *et al. THE PRESENT AND FUTURE Challenges in Infective Endocarditis*.
466 (2017).

467 6. Yoganathan, A. P., He, Z. & Casey Jones, S. Fluid Mechanics of Heart Valves. *Annu Rev*
468 *Biomed Eng* **6**, 331–362 (2004).

469 7. Secchi, E. *et al.* The effect of flow on swimming bacteria controls the initial colonization
470 of curved surfaces. *Nat Commun* **11**, (2020).

471 8. Lecuyer, S. *et al.* Shear Stress Increases the Residence Time of Adhesion of Pseudomonas
472 aeruginosa. *Biophys J* **100**, 341–350 (2011).

473 9. Sanfilippo, J. E. *et al.* Microfluidic-based transcriptomics reveal force-independent
474 bacterial rheosensing. *Nature Microbiology* vol. 4 1274–1281(2019).

475 10. Mathijssen, A. J. T. M., Shendruk, T. N., Yeomans, J. M. & Doostmohammadi, A.
476 Upstream Swimming in Microbiological Flows. *Phys Rev Lett* **116**, 28104 (2016).

477 11. Park, A., Jeong, H. H., Lee, J., Kim, K. P. & Lee, C. S. Effect of shear stress on the
478 formation of bacterial biofilm in a microfluidic channel. *Biochip J* **5**, 236–241 (2011).

479 12. Drescher, K., Shen, Y., Bassler, B. L. & Stone, H. A. Biofilm streamers cause catastrophic
480 disruption of flow with consequences for environmental and medical systems. *Proc Natl*
481 *Acad Sci U S A* **110**, 4345–4350 (2013).
482 13. Rusconi, R., Lecuyer, S., Guglielmini, L. & Stone, H. A. Laminar flow around corners
483 triggers the formation of biofilm streamers. *J R Soc Interface* **7**, 1293–1299 (2010).
484 14. Cremer, J. *et al.* Effect of flow and peristaltic mixing on bacterial growth in a gut-like
485 channel. *Proc Natl Acad Sci U S A* **113**, 11414–11419 (2016).
486 15. Rath, H., Stumpp, S. N. & Stiesch, M. Development of a flow chamber system for the
487 reproducible in vitro analysis of biofilm formation on implant materials. *PloS One* **12**,
488 e0172095- (2017).
489 16. Guttenplan, S. B., Blair, K. M. & Kearns, D. B. The EpsE Flagellar Clutch Is Bifunctional
490 and Synergizes with EPS Biosynthesis to Promote Bacillus subtilis Biofilm Formation.
491 *PloS Genet* **6**, e1001243- (2010).
492 17. Lele, P. P., Hosu, B. G. & Berg, H. C. Dynamics of mechanosensing in the bacterial
493 flagellar motor. *Proceedings of the National Academy of Sciences* **110**, 11839–11844
494 (2013).
495 18. Siryaporn, A., Kuchma, S. L., O'Toole, G. A. & Gitai, Z. Surface attachment induces
496 Pseudomonas aeruginosa virulence. *Proceedings of the National Academy of Sciences*
497 **111**, 16860–16865 (2014).
498 19. Martínez-García, R., Nadell, C. D., Hartmann, R., Drescher, K. & Bonachela, J. A. Cell
499 adhesion and fluid flow jointly initiate genotype spatial distribution in biofilms. *PloS*
500 *Comput Biol* **14**, e1006094- (2018).

501 20. Liesenborghs, L. *et al.* Staphylococcus aureus endocarditis: distinct mechanisms of
502 bacterial adhesion to damaged and inflamed heart valves. *Eur Heart J* **40**, 3248–3259
503 (2019).
504 21. Sauer, M. M. *et al.* Catch-bond mechanism of the bacterial adhesin FimH. *Nat Commun* **7**,
505 (2016).
506 22. Jung, C. J. *et al.* Endocarditis pathogen promotes vegetation formation by inducing
507 intravascular neutrophil extracellular traps through activated platelets. *Circulation* **131**,
508 571–581 (2015).
509 23. Thuny, F., Grisoli, D., Collart, F., Habib, G. & Raoult, D. Management of infective
510 endocarditis: challenges and perspectives. *The Lancet* **379**, 965–975 (2012).
511 24. Pettersson, G. B. *et al.* 2016 The American Association for Thoracic Surgery (AATS)
512 consensus guidelines: Surgical treatment of infective endocarditis: Executive summary. *J*
513 *Thorac Cardiovasc Surg* **153**, 1241-1258.e29 (2017).
514 25. Omran, A. S., Arifi, A. A. & Mohamed, A. A. Echocardiography in mitral stenosis. *J*
515 *Saudi Heart Assoc* **23**, 51–58 (2011).
516 26. Fuchs, A. *et al.* Normal values of left ventricular mass and cardiac chamber volumes
517 assessed by 320-detector computed tomography angiography in the Copenhagen General
518 Population Study. *Eur Heart J Cardiovasc Imaging* **17**, 1009–1017 (2016).
519 27. Mukherjee, S. & Bassler, B. L. Bacterial quorum sensing in complex and dynamically
520 changing environments. *Nature Reviews Microbiology* vol. 17 371–382 (2019).
521 28. Kirisits, M. J. *et al.* Influence of the hydrodynamic environment on quorum sensing in
522 Pseudomonas aeruginosa biofilms. In *Journal of Bacteriology* vol. 189 8357–8360 (2007).

523 29. Purevdorj, B., Costerton, J. W. & Stoodley, P. Influence of hydrodynamics and cell
524 signaling on the structure and behavior of Pseudomonas aeruginosa biofilms. *Appl*
525 *Environ Microbiol* **68**, 4457–4464 (2002).
526 30. Kim, M. K., Ingremeau, F., Zhao, A., Bassler, B. L. & Stone, H. A. Local and global
527 consequences of flow on bacterial quorum sensing. *Nat Microbiol* **1**, (2016).
528 31. Boles, B. R. & Horswill, A. R. agr-Mediated Dispersal of Staphylococcus aureus
529 Biofilms. *PloS Pathog* **4**, e1000052- (2008).
530 32. Yarwood, J. M., Bartels, D. J., Volper, E. M. & Greenberg, E. P. Quorum Sensing in
531 Staphylococcus aureus Biofilms. *J Bacteriol* **186**, 1838–1850 (2004).
532 33. Lauderdale, K. J., Malone, C. L., Boles, B. R., Morcuende, J. & Horswill, A. R. Biofilm
533 dispersal of community-associated methicillin-resistant Staphylococcus aureus on
534 orthopedic implant material. *Journal of Orthopaedic Research* **28**, 55–61 (2010).
535 34. Hancock, L. E. & Perego, M. The Enterococcus faecalis fsr two-component system
536 controls biofilm development through production of gelatinase. *J Bacteriol* **186**, 5629–
537 5639 (2004).
538 35. Saraiva, B. M. *et al.* Reassessment of the distinctive geometry of Staphylococcus aureus
539 cell division. *Nat Commun* **11**, (2020).
540 36. Higgins, M. L. & Shockman, G. D. *Model for Cell Wall Growth of Streptococcus faecalis*.
541 *Journal of Bacteriology* vol. 101 https://journals.asm.org/journal/jb (1970).
542 37. Persat, A., Inclan, Y. F., Engel, J. N., Stone, H. A. & Gitai, Z. Type IV pili
543 mechanochemically regulate virulence factors in Pseudomonas aeruginosa. *Proc Natl*
544 *Acad Sci USA* **112**, 7563–7568 (2015).

545 38. Webster, S. S. *et al. Force-Induced Changes of PilY1 Drive Surface Sensing by*
546 *Pseudomonas aeruginosa*. https://journals.asm.org/journal/mbio (2022).
547 39. Lister, J. L. & Horswill, A. R. Staphylococcus aureus biofilms: Recent developments in
548 biofilm dispersal. *Front Cell Infect Microbiol* **4**, (2014).
549 40. Fernandez, N. L. *et al.* Vibrio cholerae adapts to sessile and motile lifestyles by cyclic di-
550 GMP regulation of cell shape. Doi:10.1073/pnas.2010199117/-/DCSupplemental.
551 41. Keshavarz, T., Walker, M. M., Karim, Q. N., Sidebotham, R. L. & Worku, M. L. The
552 relationship between Helicobacter pylori motility, morphology and phase of growth:
553 implications for gastric colonization and pathology. *Microbiology (N Y)* **145**, 2803–2811
554 (1999).
555 42. Persat, A., Stone, H. A. & Gitai, Z. The curved shape of 30aulobacter crescentus enhances
556 surface colonization in flow. *Nat Commun* **5**, (2014).
557 43. Castellana, M. *et al.* Enzyme clustering accelerates processing of intermediates through
558 metabolic channeling. *Nat Biotechnol* **32**, 1011–1018 (2014).
559 44. Hallinen, K. M., Guardiola-Flores, K. A. & Wood, K. B. Fluorescent reporter plasmids for
560 single-cell and bulk-level composition assays in E. faecalis. *PloS One* **15**, e0232539-
561 (2020).
562 45. Zhao, A. *et al.* Reconstitution of the S. aureus agr quorum sensing pathway reveals a
563 direct role for the integral membrane protease MroQ in pheromone biosynthesis. (2022)
564 doi:10.1073/pnas.
565 46. McBrayer, D. N., Gantman, B. K., Cameron, C. D. & Tal-Gan, Y. An Entirely Solid Phase
566 Peptide Synthesis-Based Strategy for Synthesis of Gelatinase Biosynthesis-Activating
567 Pheromone (GBAP) Analogue Libraries: Investigating the Structure-Activity

568 Relationships of the Enterococcus faecalis Quorum Sensing Signal. *Org Lett* **19**, 3295–
569 3298 (2017).
570 47. Rudin, L., Sjostr6m, J.-E., Lindberg, M. & Philipson, L. *Factors Affecting Competence for*
571 *Transformation in Staphylococcus aureus*. *Journal of Bacteriology* vol. 118
572 https://journals.asm.org/journal/jb (1974).

Supplementary Information is available for this paper.

Acknowledgements: We thank members of the Gitai Lab, Josh Shaevitz, and members of the Shaevitz lab for discussion and feedback. This work was supported by grant MCB 2033020 from the National Science Foundation (to ZG and HAS). Additional funding came from the National Science Foundation PHY-1734030 (KMH).

Author Contributions: K.M.H. and Z.G. designed the experiments. K.M.H. performed the experiments and conducted image analysis. S.P.B. and T.W.M. provided the small molecules used in this study. K.M.H., H.A.S., and N.S.W. developed the computational models. K.M.H. and Z.G. wrote the paper with input from all authors.

Competing Interests: The authors declare no competing interests.

Corresponding Author: Correspondence and requests for materials should be addressed to Z.G.

588 ***Supplementary Information***

589 ***S. aureus* transport effect captured in a model of ODEs**

590 To incorporate the dynamics of QS systems and transport of signaling molecules, we developed
591 a model of coupled ODEs, describing cell number and growth (Eq. 1) and production and
592 transport of the signaling molecule (Eq. 2). For the number of cells n, we use

593

594 $$\frac{dn}{dt} = gn(t) + \beta \frac{c^h}{c^h + K^h} n(t) + an(t) - rn(t) \qquad \text{Eq. 1}$$

595

596 where, t is time, g is the cellular growth rate, β is the dispersal constant, c is the concentration of
597 the autoinducer signaling molecule, a is the rate of attachment of new cells, and r is the quorum
598 sensing-independent detachment of cells. We note a and r experimentally appear to be negligible
599 (see Movie S9: dynamics of *S. aureus* in the absence of growth) and were thus set to 0 for our
600 model simulations. We use a Hill function to describe the dynamics of the QS system, as a
601 function of the signaling molecule concentration. Here, K is the half maximal concentration and
602 h is the Hill coefficient. As the shape of the QS response is system specific, we modeled a range
603 of h values with both positive and negative β (Fig. S2). We note the overall behavior is
604 qualitatively insensitive to the precise value of h. In the main text, we use $h = 3$ to describe the
605 positive feedback that is characteristic of QS systems. Also, for autoinducer concentration c we
606 use

607

608 $$\frac{dc}{dt} = pn(t) - qc(t) - Dc(t) \qquad \text{Eq. 2}$$

609

610 where p as the production rate of the molecule, q is the transport rate of the molecule (analogous
611 to our flow rate), and D represents the diffusion away from the colony. For our simulations, we
612 assume $D << q$ and set D to 0. The parameters used for simulations of this model can be found
613 in Table S1.
614
615 **Model describing forces on a chain mimics *E. faecalis* flow dynamics**
616 To probe the mechanical effects of flow on *E. faecalis* cell chains, we created a computational
617 model of *E. faecalis* chains in flow modeling a spring force between the cells, a bending energy
618 keeping the cells in line, and a drag force accounting for flow. To determine the different
619 responses in low and high flow, we ran simulations where the only difference in conditions was
620 the drag force: this force was 10x larger in high flow simulations, to account for the 10x larger
621 flow rate in high flow experiments.
622
623 Our agent-based model describing the mechanics-dependent colonization of *E. faecalis* was
624 written in MATLAB. Each simulated chain was initialized to a random length between one and
625 five cells long, with cells, considered simply as vertices in the chain, connected to their
626 neighbors by a stiff harmonic spring with spring constant k_s. For chains of two cells or more, the
627 subsequent cells were initialized at an angle 45° from the surface, with this angle allowed to
628 fluctuate during the simulations. The chain length also "grows" by the addition of one cell at the
629 end of the chain, initialized in line with the existing chain, after a set number of timesteps.
630 Following initialization, at each timestep the cells are moved based on the forces acting upon
631 them. There are three forces we model: the spring force between each pair of cells acting in both
632 the x and y direction, a drag force which is proportional to the shear rate and the height of the cell

633 above the surface acting in the *x* direction, and a derivative of the bending energy that tends to
634 keep the cells in a roughly straight line, again acting in both the *x* and *y* directions. Based on
635 these calculated forces, the *x* and *y* positions of the cells are updated, followed by checking for
636 surface attachment/detachment and chain breakages. For attachment, the probability of
637 attachment of each cell increases linearly as it gets closer to the surface. If a cell is already
638 attached, at each step it is checked for detachment, with the probability of detaching increasing
639 as a function of the total height of the two neighbor cells to the attached cell. Detachment of the
640 origin cell in a chain was seen rarely experimentally and this detachment event was modeled as a
641 stochastic process. If the origin cell detaches and no other cells in the chain are attached, the
642 simulation is stopped and the chain is marked as both origin and distal detached. To model
643 breakages, at each step the tension of the spring between each pair of cells is calculated. If the
644 spring tension is larger than a set value, it has a breakage probability that increases exponentially
645 with increasing spring length. Following a breakage along the chain, cells on each side of the
646 breakage are checked for attachment. If any cells in the segment of the origin cell are attached,
647 "origin segment attachment" is recorded. Similarly, if any cells on the distal chain segment are
648 attached, "distal segment attachment" is recorded.
649
650 At each time step, the cell positions were updated according to the deterministic forces (detailed
651 below) plus a small stochastic force in both *x* and *y* directions, sampled from Gaussian
652 distributions centered around 0 with a standard deviation of 0.1. We note that if updating the cell
653 positions would cause any cell to move to a negative *y* position, the cell was set to the surface
654 plus a small positive gaussian step (from a distribution of mean 0 and standard deviation 0.1).
655 After updating the position, each cell was checked for attachment, then detachment. If

656 detachment occurred, the new *y* position was similarly set to a small gaussian step above the
657 surface (from a distribution of mean 0 and standard deviation 0.01). Following these updates,
658 chains were checked for breakages, before moving to the next time step. The results of 100
659 chains, simulated in either the low flow or high flow condition, were combined to mimic the
660 corresponding flow experiment.
661
662 Regarding the spring forces on the cells in more detail, given three cells at positions *i*-1, *I,* and
663 *i*+1 connected to each other with springs, the potential energy stored in the spring connecting the
664 cell at position *I* to the cell at position *i*-1 is:
665

666 $$E_{\mathrm{s}} = \frac{1}{2} k_{\mathrm{s}} \left(\sqrt{(x_i - x_{i-1})^2 - (y_i - y_{i-1})^2} - l_0 \right)^2, \qquad \text{Eq. 3}$$

667 where k_{s} is the spring constant, *x* is the *x*-position of the cell at *I* or *i*-1, respectively, and *y*
668 similarly is the *y*-position of the cell at *I* or *i*-1, and l_0 is the unstretched length of the spring. The
669 energy of the spring connecting cell *I* to cell *i*+1, is given by the same expression, just replacing
670 the *i*-1 subscripts with *i*+1. The total spring force in *x* or *y* is then found by taking the derivative
671 of the two energy expressions with respect to x_i and y_i and summing the *x* or *y* expressions,
672 respectively.

673 The bending energy acting on the cell at position *i* which makes an angle θ with the cells at
674 positions *i*-1 and *i*+1 is given by the expression:

675 $$U_{\mathrm{b}}(\theta) = k_{\mathrm{b}}[1 + \cos\theta], \qquad \text{Eq. 4}$$

676 where k_{b} is a bending constant. This expression can be rewritten in terms of the vectors $\vec{v}_{i,i-1}$

677 and $\vec{v}_{i,i+1}$, where these are the vectors from position *i* to position *i*-1 and position *i* to position

678 *i*+1, respectively:

679 $$U_{\mathrm{b}}(\theta) = k_{\mathrm{b}}\left[1 + \frac{\vec{v}_{i,i-1}\cdot\vec{v}_{i,i+1}}{\|\vec{v}_{i,i-1}\|\|\vec{v}_{i,i+1}\|}\right]. \qquad \text{Eq. 5}$$

680 Taking the derivative of this expression with respect to x_i and y_i, x_{i-1} and y_{i-1}, and x_{i+1} and

681 y_{i+1}, gives the total bending force acting on the three cells due to the angle formed by cells *i*-1, *i*,

682 and *i*+1.

683 We approximate the force from the flow condition as a drag force that acts in the *x* direction and

684 depends on the height of the cell above the surface:

685 $$F_{\mathrm{drag},i} = d * f * y_i\,\hat{x} \qquad \text{Eq. 6}$$

686 where d is a constant, set to 1 for our simulations, *f* is the flow rate and y_i is the *y* position of cell

687 *i*. The parameters and probabilities used in simulations of our chains in low and high flow

688 conditions can be found in Tables S2 and S3, respectively.

689

690 ***S. aureus* attachment/detachment analysis**

691 To observe the amount of spontaneous detachment within our channels, as well as attachment

692 from upstream detachment, we performed an experiment in which *S. aureus* was observed in

693 flow in conditions that prevented cell growth (Movie S9). Specifically, we used a minimal

694 growth media AAM[47] but without the addition of glucose that is normally added to AAM. In

695 these experiments we observed only rare detachment and attachment events, did not see clustered

696 morphologies, and did not see dispersal events, indicating that all of these dynamic responses
697 rely on growth.
698
699 **Calculation of shear rate**
700 Microfluidic channels used in this study had a rectangular cross section. We calculated the shear
701 rate (γ) at the floor and ceiling of the channel, where height is << width, using the equation:
702
703 $$\gamma = \frac{6Q}{wh^2}, \qquad \text{Eq. 7}$$
704
705 where Q is the total flow rate, w is the width of the channel and h is the channels height.
706
707 Estimates of the shear rate in a heart valve was obtained for a channel with a circular cross
708 section. For a circular channel, the shear rate (γ) along the wall is:
709
710 $$\gamma = \frac{4Q}{\pi r^3}, \qquad \text{Eq. 8}$$
711
712 where Q is again the total flow rate and r is the radius of the cross section.
713
714 We estimated the flow rate and radius of the cross section of a valve in the heart from values
715 given in [25,26]. Focusing on values for the mitral valve, we estimate during a heartbeat that all of
716 the fluid from the left atrium passes through the valve. The average volume of the left atrium for
717 males is reported to be 81 ± 18 ml and for women to be 67 ± 14 ml. For our calculation of an
718 "average" person, we estimated the volume passing though the valve to be 75 ml. We assume a

resting heart rate of about 65 beats per minute, meaning the left atrium volume would pass through the valve in at most ~0.92 seconds. This gives a flow rate, Q, of 75 ml/0.92 s, or 81.25 cm^3/s. To determine the radius, it was reported that the mitral valve has a surface area of 4-6 cm^2. We assume the cross-sectional area of the valve is slightly larger than the cross-sectional area the fluid passes through, as the tissue making up the valve leaflets would block some of the area. We estimated a cross-sectional area of the opening for the fluid to be ~3 cm^2. We can calculate the radius of this area using the equation for the area of a circle, finding r = 0.98 cm. Putting these values of r and Q into Equation 8, we find:

$$\gamma = \frac{4Q}{\pi r^3} = \frac{4*81.25\frac{\text{cm}^3}{\text{s}}}{\pi(0.98\text{ cm})^3} = 109.9\ /\text{s}. \qquad \text{Eq. 9}$$

With this value, we roughly estimate the shear rate in valves to be around 100/s, though we do acknowledge we are assuming constant flow and a circular valve cross section.

Supplemental Tables

Transport-dependent colonization model: Parameters

	$\beta < 0$	$\beta > 0$
g	0.5	0.8
β	-1	1
h	3	3
K	45	45
p	5	5
q	[0.4, 4]	[4,40]
c_o	0	0
n_o	1	5

Table S1. *Parameters used for the transport-dependent colonization model. We note that the rates of attachment of new cells (a) and quorum sensing-independent detachment (r) as well as diffusion away from the colony (D) are set to 0.*

Mechanics-dependent colonization model: Parameters

	Parameter Values
k_s	1
l_0	1
k_b	1×10^{-3}
d	1
f	[0.001, 0.01]

Table S2. *Parameters used for the mechanics-dependent colonization model.*

Mechanics-dependent colonization model: Probabilities

	Probability	Variables and Constants
Cell attachment	$ae^{-\lambda y}$	a =0.2, $\lambda = 3$, y = height of cell above surface
Cell detachment	$ue^{-\alpha+m}$	u =1, $\alpha = 5$, m = height of neighbor cells
Origin detachment	1×10^{-6}	
Chain breakage -Check for breakage if spring tension (τ) > 0.02	$1 - be^{-\omega\tau}$	b = 1, $\omega = 0.01$, τ = spring tension

Table S3. *Probabilities used for the mechanics-dependent colonization model.*

Supplemental Figures

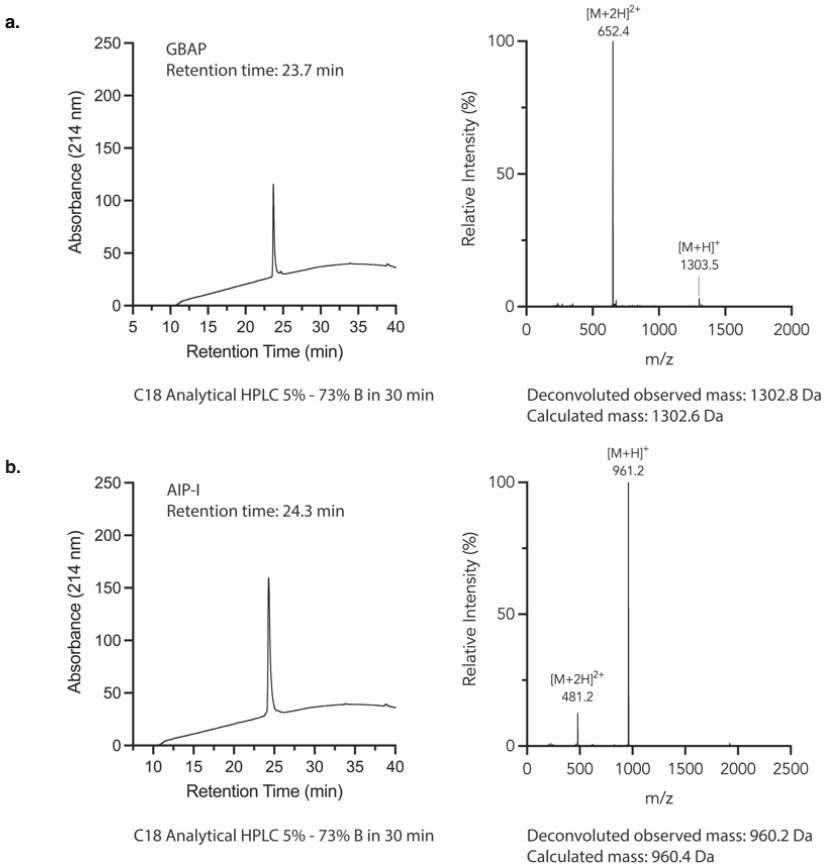

Figure S1: Characterization of synthetic autoinducing peptides
a. RP-HPLC and ESI-MS of GBAP. **b.** RPHPLC and ESI-MS of AIP-I.

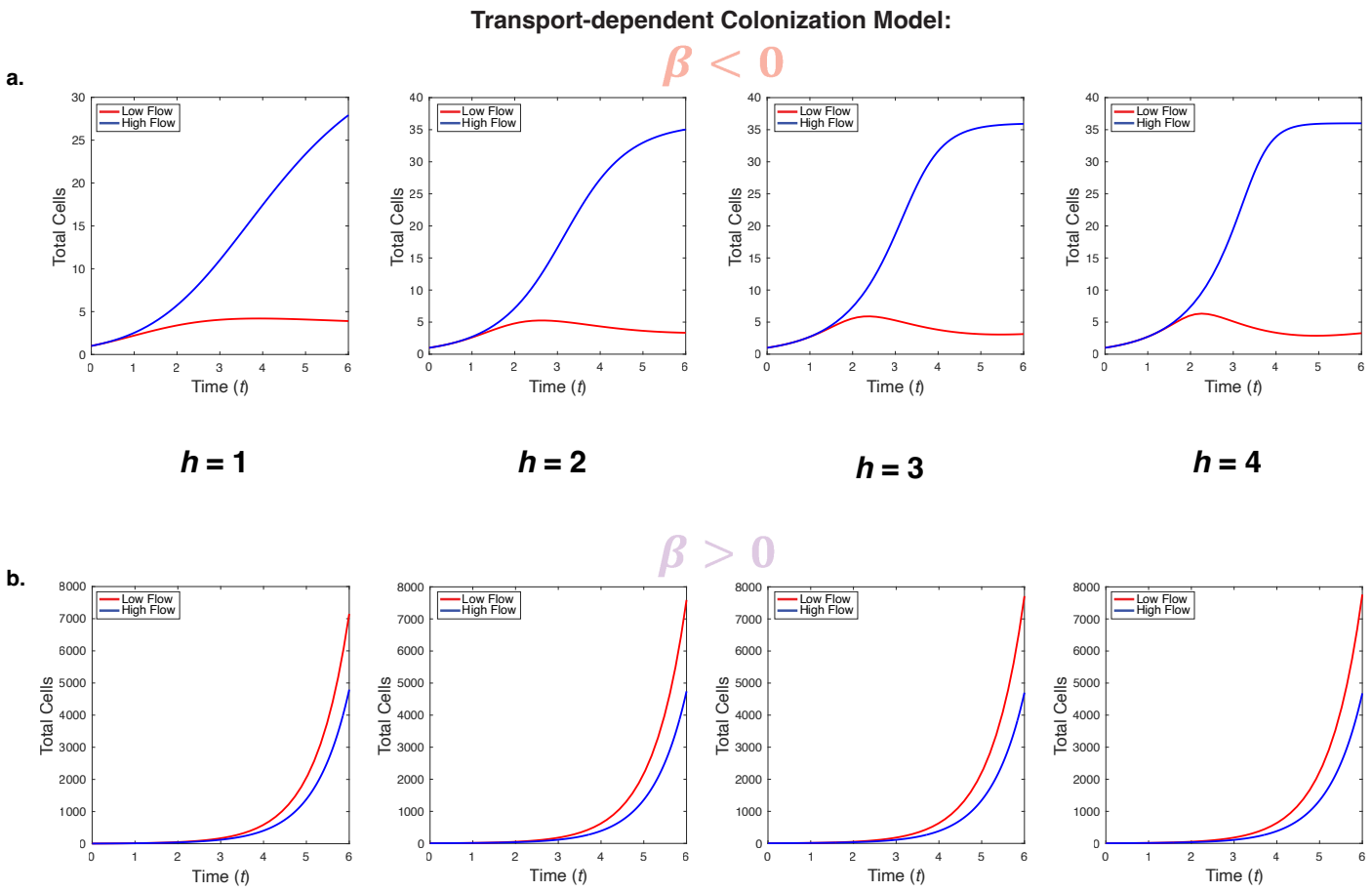

Figure S2: Varying the Hill coefficent for the transport-dependent colonization model
a. Results for our ODE transport model using a range of Hill coefficents (h=1-4, left to right) for a positive β term. In all simulations, we observe larger final cell populations in the high flow condition, compared to the low flow condition. **b.** Results for our ODE transport model using over a range of Hill coefficents (h=1-4, left to right) for a negative β term. Once again, the qualitative behavior is consistent across all choices of h, indicating the insensitivity to the specific value chosen for the Hill coefficient. For all modeling in Fig. 2, we used h=3.

Figure 1: Paradoxical final cell population in low versus high flow

a. Schematic of microfludic flow chamber used for all flow experiments. A PDMS microfluidic channel is bonded to a glass coverslip. Following cell loading, a syringe pump is turned on, flowing fresh media through the channel. Cells attached to the coverslip are imaged. **b.** Analysis of doubling times for each *S. aureus* MRSA and *E. faecalis* in low (red) and high (blue) flow conditions. **c.** Representative images of *S. aureus* MRSA at 0, 3 or 6 hours of low flow (shear rate 40/s). **d.** Similar representative images of *S. aureus* MRSA at 0, 3 or 6 hours of high flow (shear rate 400/s). **e.** Fold change of percent area covered of both low (red) and high (blue) flow experiments for *S. aureus* MRSA. **f.** Representative images of *E. faecalis* at 0, 3 or 6 hours of low flow (shear rate 40/s). **g.** Similar representative images of *E. faecalis* at 0, 3 or 6 hours of high flow (shear rate 400/s). **h.** Fold change of percent area covered of both low (red) and high (blue) flow experiments for *E. faecalis*. Image scale bars are 10 µm. Error bars are SEM.

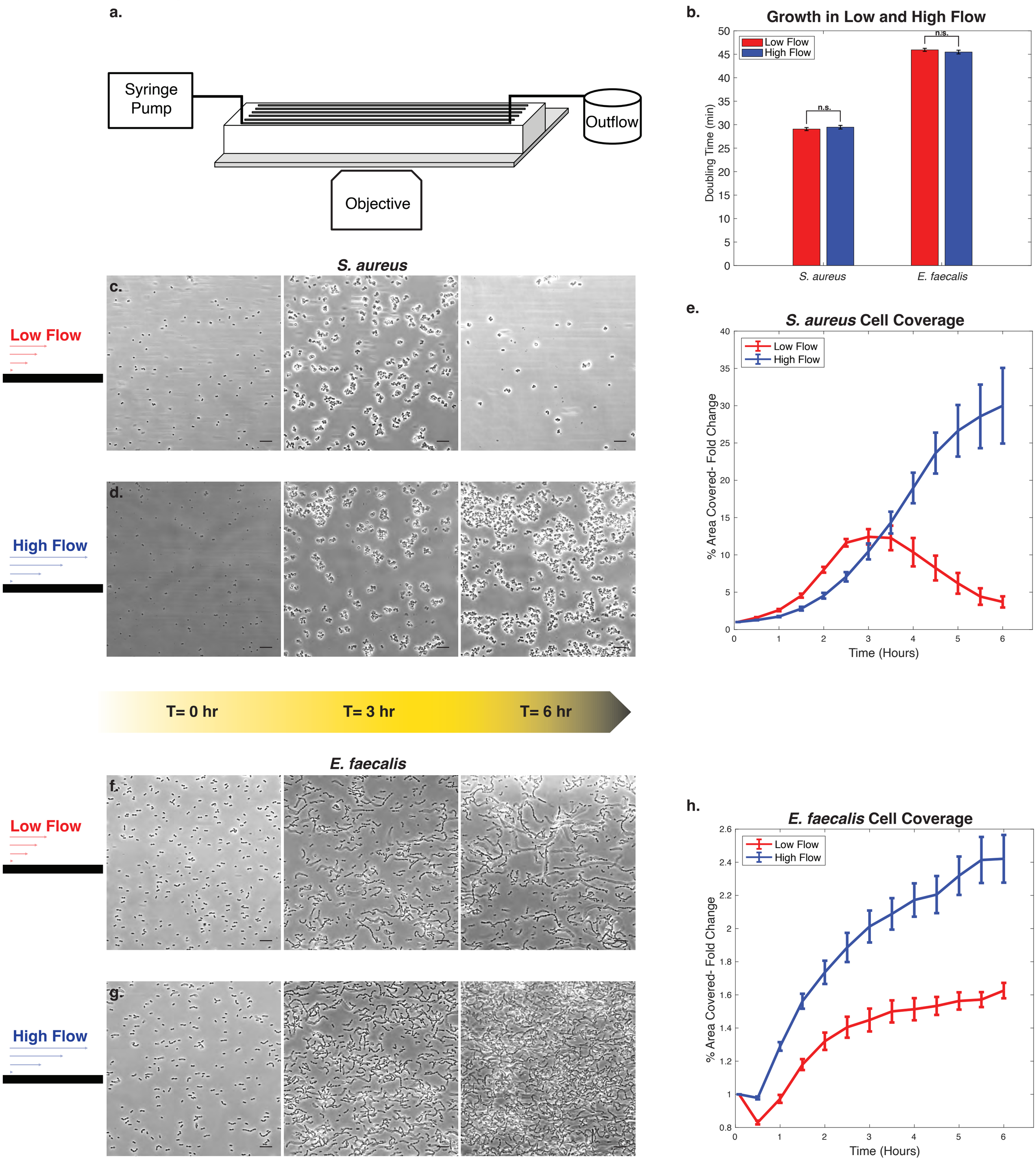

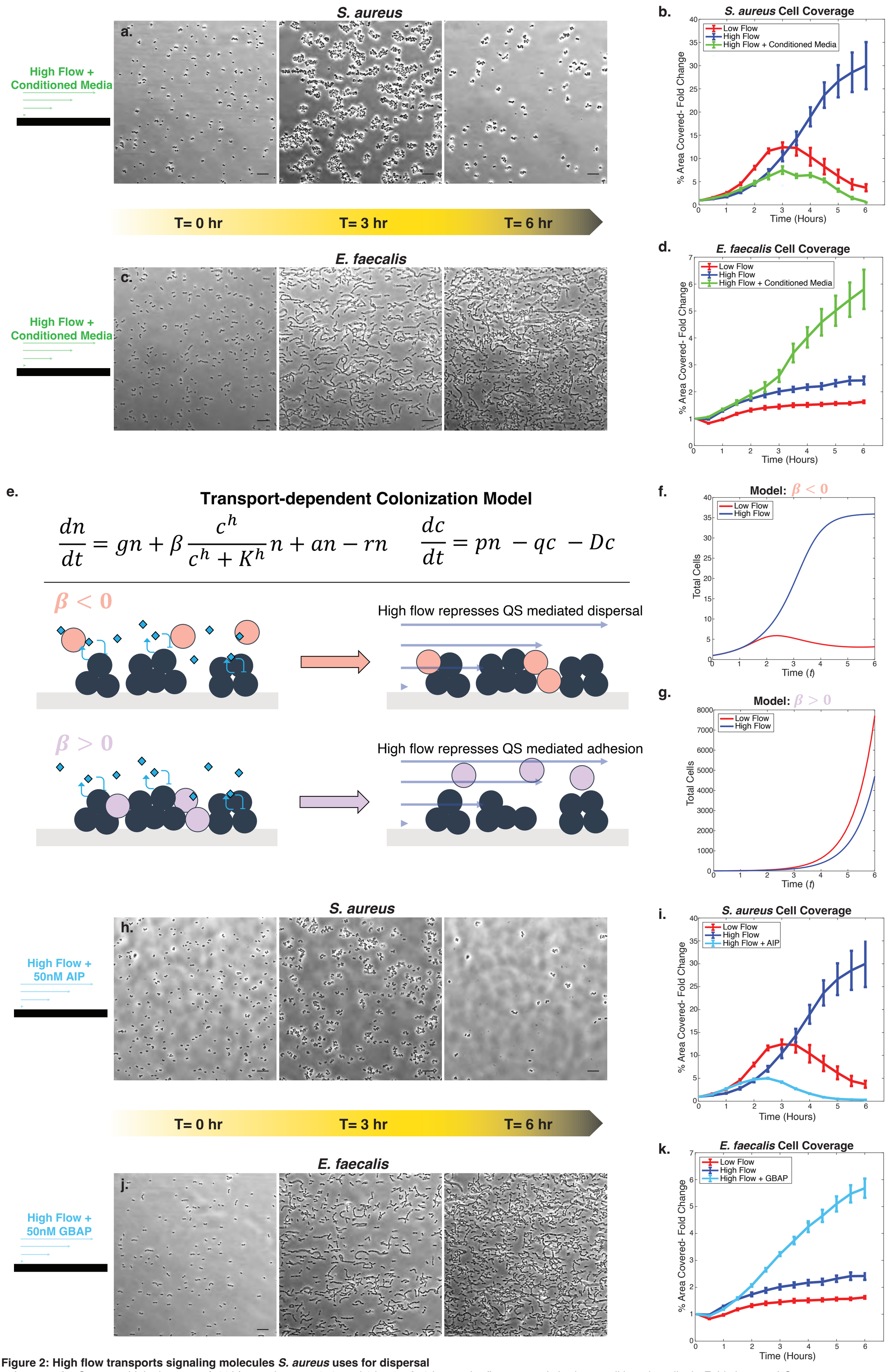

Figure 2: High flow transports signaling molecules *S. aureus* uses for dispersal

a. Images of a *S. aureus* high shear rate (400/s) experiment at 0, 3, and 6 hours. At 3 hours, the flow was switched to conditioned media. b**.** Fold change of *S. aureus* percent area covered of high + conditioned media (green) flow experiments, with initial high (blue) and low (red) flow experiments shown for comparison. **c.** Representative images of an *E. faecalis* high shear rate (400/s) experiment at 0, 3, and 6 hours, with the addition of conditioned media at the 3 hour timepoint. **d.** Fold change of *E. faecalis* percent area covered of high + conditioned media (green) flow experimens, with initial high (blue) and low (red) flow runs shown for comparison. **e.** Equations for the transport-dependent colonization model and schematic of the effects of high flow transport of signaling molecules. Depending on the sign of the β term in our model, the response under flow differs. **f.** Model prediction of dispersal in low flow with a negative β term. **g.** Model prediction of increased attachment in low flow with a positive β term. **h.** Images of *S. aureus* at 0, 3, and 6 hours of high flow (shear rate 400/s) with media supplemented with 50 nM AIP for the entire experiment. **i.** Fold change of *S. aureus* percent area covered of high + 50 nM AIP (light blue) flow experiments, with initial high (blue) and low (red) flow experiment- shown for comparison. **j.** Representative images of *E. faecalis* at 0, 3, and 6 hours of high flow (shear rate 400/s) with media supplemented with 50 nM GBAP for the entire experiment. **k.** Fold change of *E. faecalis* percent area covered of high + 50 nM GBAP (light blue) flow experimens, with initial high (blue) and low (red) flow experiments shown for comparison. Image scale bars are 10 µm. Error bars are SEM.

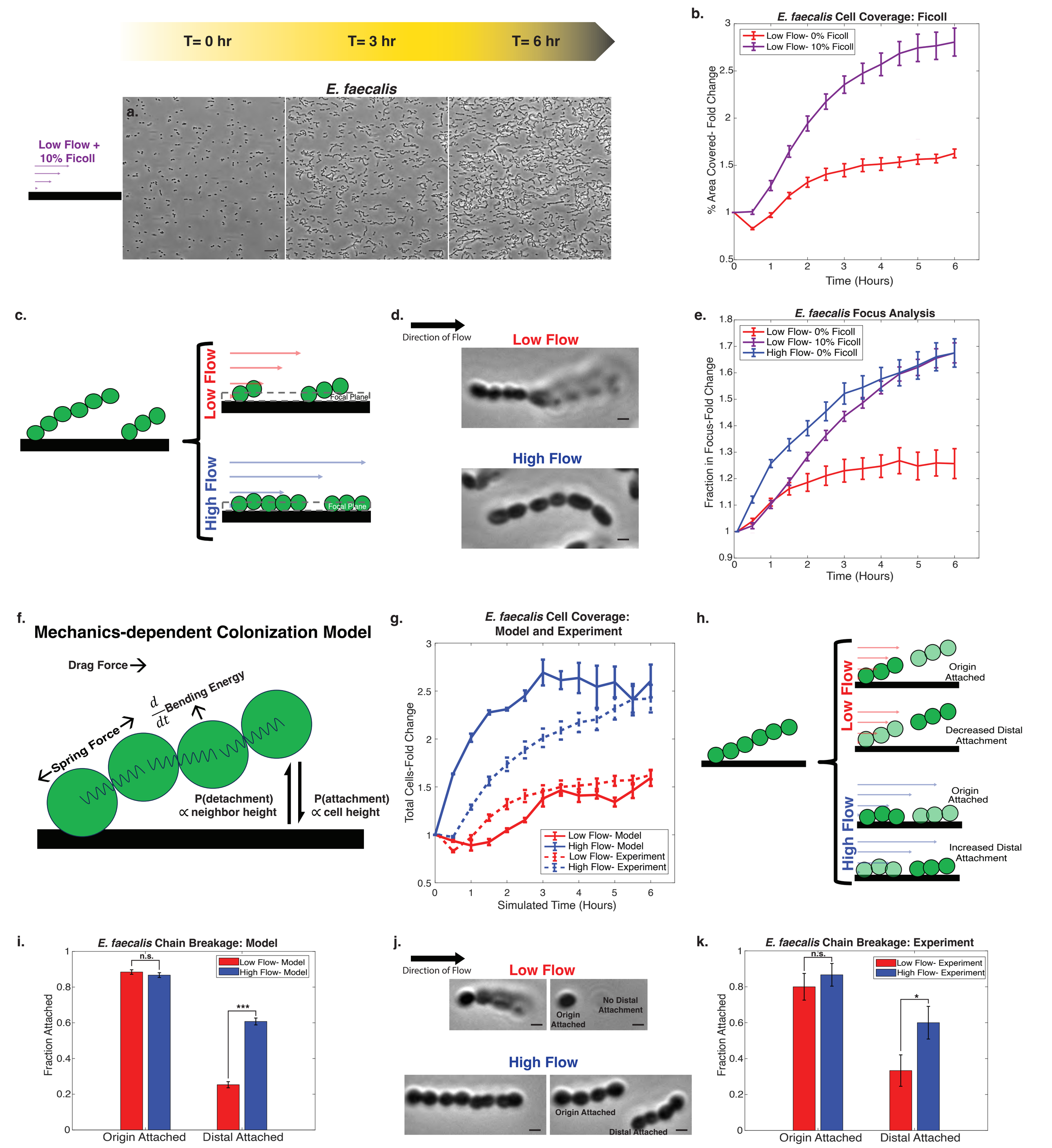

Figure 3: Mechanical dynamics of chains in flow lead to more cells attached and in focus in *E. faecalis*.
a. Representative images of a low flow *E. faecalis* experiment at 0, 3, and 6 hours with 10% ficoll added to the media. **b.** Fold change of area covered for *E. faecalis* low flow experiments with 10% ficoll (purple). Low flow with 0% ficoll is shown as red line for comparison. For flow experiement images, scale bars are 10 µm. **c.** Schematic demonstrating chain dynamics and focus plane for low versus high flow. **d.** Example chains in low flow (top) and high flow (bottom). In high flow, the chain is pushed to the surface and more individual cells are in focus. **e.** Fold change of fraction in focus for *E. faecalis* experiments of low flow with 0% ficoll (red), 10% ficoll (purple), and high flow with 0% ficoll (blue). Brightfield images were thresholded to determine fraction in focus. **f.** Schematic of the forces and attachment/detachment dynamics implemented in our mechanics-dependent colonization model. **g.** Comparison of total cell coverage from the model in low and high flow (red and blue, solid line) compared to experimental *E. faecalis* runs (red and blue, dashed line). **h.** Schematic depicting possible chain dynamics following a breakage event in low (upper two) and high (lower two) flow. **i.** Mechanics model prediction of chain breakage dynamics in low flow conditions (red) and high flow conditions (blue). Following a breakage event in the model, the anchor and distal attachments were recorded for 100 simulated chains. **j.** Experimental observations of breakage events from low flow (top), where the chain breaks and only the origin cell is still attached, and high flow (bottom), where the chain breaks and both the distal and origin cells are attached. Images shown are from two consecutive time points ($\Delta t = 5$ min). **k.** Fraction attached for both origin and distal in high and low flow experiments. Flow videos were analyzed for breakage events throughout the 6 hour experiemnt. For $n = 30$ chains in both high and low flow, the outcome after a breakage - anchor or distal adherence - was counted. We note that chains could break and have both origin and distal adhered or could completly detach from the surface, leading to neither origin nor distal adhered. P value was determined using a paired t-test. * = $p < 0.05$, *** = $p < 0.005$. Scale bars in both D and J are 1 µm. For all graphs, error bars are SEM.

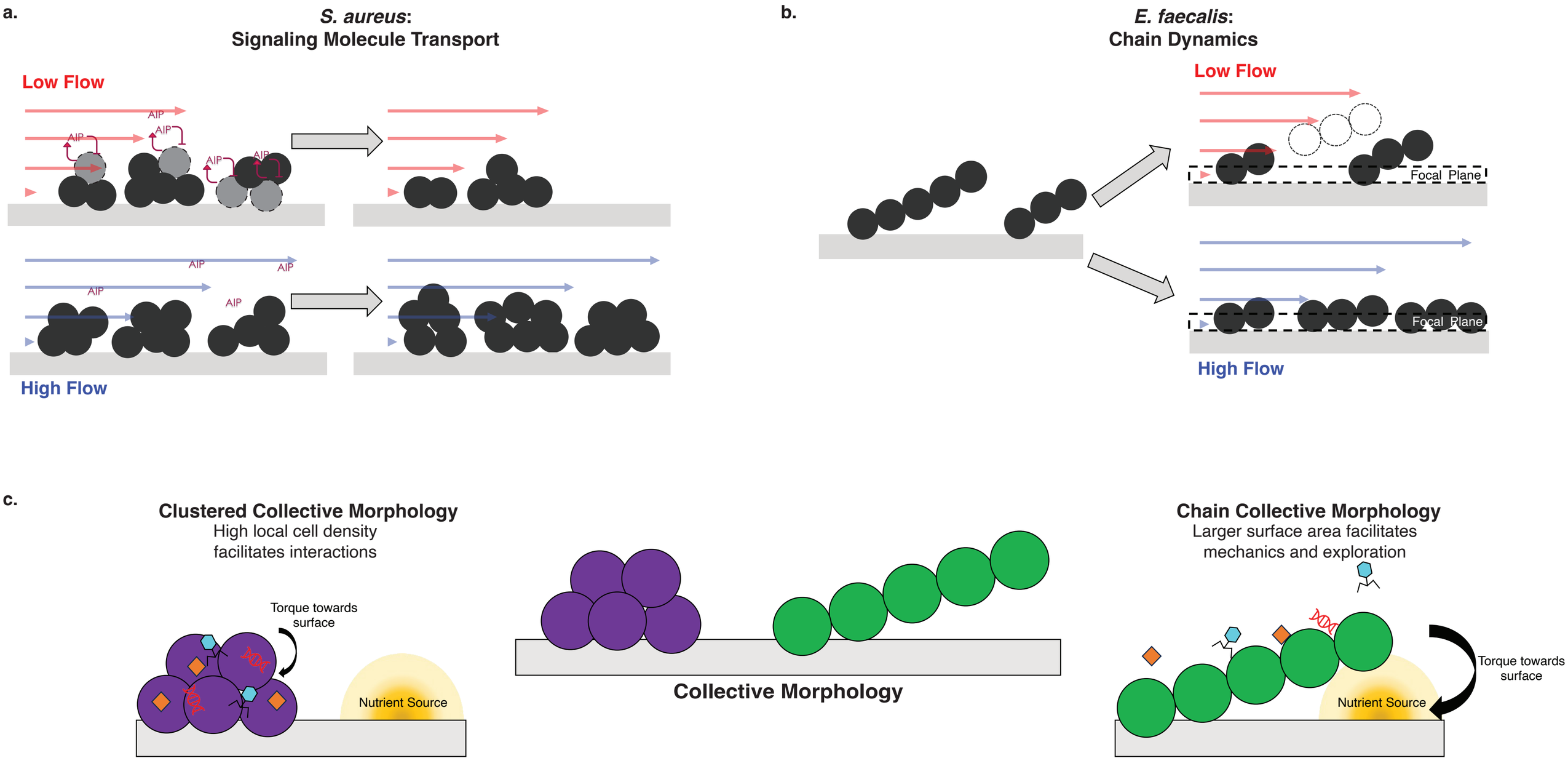

Figure 4: Divergent mechanisms drive population dynamics in flow environments of two different pathogenic species
a. Model of *S. aureus* transport effects in low and high flow. The signaling molecule (AIP) is produced in both cases but high flow transports the molecule before the QS pathway is activated. In low flow, the AIP activates QS, leading to cell dispersal from the clusters. **b.** Model of the chain mechanism in low and high flow for *E. faecalis*. In low and high flow, the flow pushes the chains towards the surface. In high flow, the larger forces lead to more cells in focus, as well as more distal cells attached after a breakage. **c.** Schematic describing the observed collective morphologies of our two species of interest. The two divergent mechanisms found for flow responses can be tied to the collective morphologies of the specific species. Implications of these morphologies may play a role in a multitude of population-level, bacterial behaviors.